

See discussions, stats, and author profiles for this publication at: <https://www.researchgate.net/publication/273326582>

# Transition fields in organic materials: From percolation to inverted Marcus regime. A consistent Monte Carlo simulation in disordered PPV

ARTICLE *in* THE JOURNAL OF CHEMICAL PHYSICS · MARCH 2015

Impact Factor: 2.95 · DOI: 10.1063/1.4913733 · Source: PubMed

---

READS

52

## 3 AUTHORS:



Riccardo Volpi

Linköping University

2 PUBLICATIONS 0 CITATIONS

[SEE PROFILE](#)



Sven Stafström

Linköping University

223 PUBLICATIONS 5,301 CITATIONS

[SEE PROFILE](#)



Mathieu Linares

Linköping University

63 PUBLICATIONS 978 CITATIONS

[SEE PROFILE](#)



## Transition fields in organic materials: From percolation to inverted Marcus regime. A consistent Monte Carlo simulation in disordered PPV

Riccardo Volpi, Sven Stafström, and Mathieu Linares

Citation: *The Journal of Chemical Physics* **142**, 094503 (2015); doi: 10.1063/1.4913733

View online: <http://dx.doi.org/10.1063/1.4913733>

View Table of Contents: <http://scitation.aip.org/content/aip/journal/jcp/142/9?ver=pdfcov>

Published by the AIP Publishing

---

### Articles you may be interested in

An improved dynamic Monte Carlo model coupled with Poisson equation to simulate the performance of organic photovoltaic devices

*J. Chem. Phys.* **134**, 124102 (2011); 10.1063/1.3569130

Hole transport in the organic small molecule material  $\alpha$ -NPD : evidence for the presence of correlated disorder

*J. Appl. Phys.* **107**, 113710 (2010); 10.1063/1.3407561

Combination of a polyaniline anode and doped charge transport layers for high-efficiency organic light emitting diodes

*J. Appl. Phys.* **101**, 124509 (2007); 10.1063/1.2748864

Mesoscale modeling of electrical percolation in fiber-filled systems

*J. Chem. Phys.* **123**, 134702 (2005); 10.1063/1.2031147

Trap concentration dependence of percolation in doped small molecule organic materials

*J. Appl. Phys.* **98**, 043511 (2005); 10.1063/1.2005378

---

## The logo for AIP | The Journal of Chemical Physics, identical to the one at the top of the page, but set against a dark blue background with a vibrant, multi-colored starburst pattern of green, purple, and yellow lines radiating from the bottom left corner.

### Meet The New Deputy Editors



Peter  
Hamm



David E.  
Manolopoulos



James L.  
Skinner

# Transition fields in organic materials: From percolation to inverted Marcus regime. A consistent Monte Carlo simulation in disordered PPV

Riccardo Volpi, Sven Stafström, and Mathieu Linares<sup>a)</sup>

*Department of Physics, Chemistry and Biology (IFM), Linköping University, SE-581 83 Linköping, Sweden*

(Received 29 October 2014; accepted 13 February 2015; published online 5 March 2015)

In this article, we analyze the electric field dependence of the hole mobility in disordered poly(p-phenylene vinylene). The charge carrier mobility is obtained from Monte Carlo simulations. Depending on the field strength three regions can be identified: the percolation region, the correlation region, and the inverted region. Each region is characterized by a different conduction mechanism and thus a different functional dependence of the mobility on the electric field. Earlier studies have highlighted that Poole-Frenkel law, which appears in the correlation region, is based on the type of correlation caused by randomly distributed electric dipoles. This behavior is thus observed in a limited range of field strengths, and by studying a broader range of electric fields, a more fundamental understanding of the transport mechanism is obtained. We identify the electric fields determining the transitions between the different conduction mechanisms in the material and we explain their physical origin. In principle, this allows us to characterize the mobility field dependence for any organic material. Additionally, we study the charge carrier trapping mechanisms due to diagonal and off-diagonal disorder, respectively. © 2015 AIP Publishing LLC. [<http://dx.doi.org/10.1063/1.4913733>]

## I. INTRODUCTION

In the last decades, organic semiconductors, and in particular polymeric materials, have attracted a huge interest among scientists. This kind of materials can be produced at low cost and they exhibit peculiar characteristics leading to new promising applications such as organic light-emitting diodes (OLEDs)<sup>1</sup> and organic solar cells.<sup>2,3</sup> Unfortunately, these devices are still not competitive with their inorganic counterparts, their efficiency as well as their stability needs to be improved. One of the main limiting effects on the transport properties, and thereby also the efficiency, is the high degree of disorder in polymeric materials. In order to account for these effects, it is important to consider a realistic structure for the polymer chains. Theoretical studies are relevant to help the trial and error process in the design of polymers<sup>4</sup> and in the understanding of their supramolecular organization.<sup>5</sup>

The conduction is due to electrons (or holes) occupying  $\pi$  orbitals that are delocalized over the backbone of the polymer chain/segment but that normally do not extend over several chains. Therefore, the charge carrier has to be transferred between polymer segments via a hopping mechanism. The hopping rates are determined from quantum mechanical probabilities derived using perturbation theory. In the case of polymer segments (or molecules), the reorganization of the constituents is an important factor and the transfer rates are normally determined from the Marcus formula.<sup>6</sup> The intrinsic probabilistic nature of the conduction combined with the structural disorder inherent to these materials makes it difficult to find an analytical expression for the conductivity. Instead, Monte Carlo (MC) simulations<sup>7</sup> can easily model these aspects. In a previous article,<sup>8</sup> we showed how simulations of

this type of systems can be performed including the true off-diagonal disorder, i.e., taking into account realistic intermolecular orientations, known to be a crucial aspect for calculating the electronic overlap between neighbors.<sup>9–12</sup> The study by Jakobsson *et al.* was focused on poly(p-phenylene vinylene) (PPV) and its bulk disordered structure was obtained by a molecular dynamics (MD) simulation at 300 K.<sup>8</sup> The results obtained in Ref. 8 are in agreement with the theoretically predicted mobility temperature dependence; however, it failed to reproduce the mobility field dependence that should follow Poole-Frenkel law in the considered range of electric fields.

The Poole-Frenkel law<sup>13</sup> was originally derived to describe dielectric breakdown and is based on ionic traps. A high concentration of such traps is very unlikely in the case of organic semiconductors. However, a similar type of energy landscape is obtained for these materials as a result of randomly distributed electric dipoles. Several studies have pointed out the close relationship between the Poole-Frenkel law and the energy landscape caused by such dipoles in organic materials,<sup>14–17</sup> in particular in the detailed work by Dunlap and co-workers.<sup>18</sup> As a model for the diagonal disorder, we consider the potential energy landscape caused by the molecular dipoles with directions coinciding with the realistic molecular directions coming out from a molecular dynamics simulation. This, in combination with the off-diagonal disorder caused by the dependence of transfer integrals on the relative orientation between molecular pairs will give us a detailed insight into the field dependence of the hole mobility in PPV.

## II. THEORY

In this section, we will briefly present the theoretical background inspiring our simulations. This section is written here

<sup>a)</sup>[mathieu@ifm.liu.se](mailto:mathieu@ifm.liu.se)

for reader convenience and it follows in its general overview, Ref. 18.

When the disorder of the system is very large, some molecular sites act as deep traps, i.e., the time a charge spends on one of these sites is very long compared to the time spent traveling in between them. In this situation, the transport of the charge carriers is mainly limited by the critical traps, defined as the traps with the largest average escape times. The mobility can be expressed as

$$\mu \sim \frac{\langle d \rangle}{\langle \tau \rangle E}, \quad (1)$$

where  $\langle d \rangle$  is the average distance between two critical traps,  $\langle \tau \rangle$  is the average escape time from a critical trap, and  $E$  is the applied electric field. Assuming that the charge moves in the direction of the field, the average escape time decreases with increasing field strength and is proportional to

$$\langle \tau \rangle \sim \exp\left(\frac{\Delta - eEr_c}{k_B T}\right), \quad (2)$$

where  $\Delta$  and  $r_c$  are the depth and width (from bottom to rim) of the critical traps, respectively. Substituting (2) in (1), the mobility dependence on the field becomes

$$\mu \sim \frac{1}{E} \exp\left(\frac{eEr_c}{k_B T}\right), \quad (3)$$

an expression that is valid in the range in which the above assumptions are true, i.e., the correlation region. In this region, indeed the spatial energetic correlation in the material is ruling the conduction mechanism, through the critical radius  $r_c$  in formula (3).

For uncorrelated disorder, the critical traps are single sites with exceptionally low energy compared to their neighbors and thus we can assume  $r_c \approx a$ , the average nearest neighbors distance. This condition, together with (3), results in the following expression for the mobility:

$$\ln \mu \sim \frac{eEa}{k_B T} - \ln E. \quad (4)$$

For correlated energy landscapes, instead, there is a correlation between the width and the depth of a trap. The landscape is spatially smoother, passing gradually (not suddenly) from one extreme to the other of the density of states (DOS). In the case of randomly distributed interacting dipoles, it has been demonstrated in the literature<sup>19,20</sup> that the energy distribution (density of states) is approximately a gaussian and the spatial correlation is proportional to  $1/r$ ,

$$\langle u(0)u(r) \rangle = \sigma^2 \frac{a_d}{r}, \quad (5)$$

where  $\sigma$  is the standard deviation of the DOS of the system and  $a_d$  is the characteristic radius depending on the material arrangement and on the electrostatic interaction. Knowing that the difference between two random variables having a gaussian distribution results in a new variable also having a gaussian distribution, we can characterize the distribution of the energy difference  $\Delta(r) = u(r) - u(0)$  at a distance  $r$  by simply calculating its variance  $\Sigma(r)^2$ . Using (5), we obtain

$$\Sigma(r)^2 = \langle \Delta(r)^2 \rangle = 2\sigma^2 \left(1 - \frac{a_d}{r}\right). \quad (6)$$

Rewriting Eq. (2) as a function of  $r$ , the average escape time from a valley of radius  $r$  is

$$\langle \tau(r) \rangle = \tau_0 \left\langle \exp\left(-\frac{eEr}{k_B T} + \frac{\Delta(r)}{k_B T}\right) \right\rangle. \quad (7)$$

Averaging with the gaussian probability density  $P(\Delta; r)$  with zero mean and variance given by (6), we arrive at

$$\langle \tau(r) \rangle = \tau_0 \exp\left(-\frac{eEr}{k_B T} + \frac{\Sigma(r)^2}{2(k_B T)^2}\right). \quad (8)$$

The average escape time in (8) as function of  $r$  has a maximum when the exponent is maximum, i.e., when

$$\frac{d}{dr} \left( -\frac{eEr}{k_B T} + \left(\frac{\sigma}{k_B T}\right)^2 \left(1 - \frac{a_d}{r}\right) \right) = 0 \quad (9)$$

and the critical traps are thus those with radius given by solving (9),

$$r_c = \sigma \sqrt{\frac{a_d}{eEk_B T}}. \quad (10)$$

Due to the energy correlation, when the field tends to 0, the critical traps become infinitely wide ( $E \rightarrow 0, r_c \rightarrow \infty$ ). Now, assuming an infinite system so that we can always find a sufficient number of critical traps to dominate the conduction process, we obtain the mean critical traps escape time as

$$\langle \tau \rangle = \tau_0 \exp\left(\left(\frac{\sigma}{k_B T}\right)^2 - 2\left(\frac{\sigma}{k_B T}\right)^{\frac{3}{2}} \sqrt{\frac{eEd_a}{\sigma}}\right). \quad (11)$$

Substituting this expression into (1), we obtain the following functional dependence of the mobility:

$$\mu = \frac{\langle d \rangle}{\langle \tau_0 \rangle E} \exp\left(-\left(\frac{\sigma}{k_B T}\right)^2 + \gamma \sqrt{E}\right), \quad (12)$$

also known as Poole-Frenkel dependence.<sup>13</sup>

So, as briefly summarized in this section, Poole-Frenkel is a result of dipole correlation and should not be observed in uncorrelated gaussian disordered models (GDMs) as in Ref. 21, except for a restricted electric field range. To observe it, we will have to introduce molecular dipoles in our system and consider their electrostatic interactions with the charge carriers.

### III. METHOD

We model the PPV chain segments with an atomistic description of 4 units oligomers (4PV), arranged in a box composed of 22 500 oligomers whose approximate size is  $24 \times 24 \times 24 \text{ nm}^3$ . The charge carrier is occupying a 4PV molecular orbital, being delocalized over the whole molecule. This choice is appropriate considering the limited charge delocalization length in PPV.

The construction of the 4PV box and its evolution through MD simulation have been described in our previous work.<sup>8</sup> Molecular dynamics simulations in the NPT ensemble were performed during 3 ns using the OPLS (optimized potentials for liquid simulations) force field<sup>22,23</sup> and the GROMACS program<sup>24-27</sup> with periodic boundary conditions (PBCs). The

temperature was maintained at 300 K using a Nosé-Hoover thermostat<sup>28,29</sup> with a coupling constant of 0.2 ps. The pressure was maintained at 1 atm using the Parrinello-Rahman barostat<sup>30,31</sup> with a coupling constant of 0.2 ps. The cutoff distance applied for both electrostatic and van der Waals interactions was 1.5 nm. After equilibration, the 4PV box converged to size  $24.2 \times 24.2 \times 24.2 \text{ nm}^3$  and density  $1083 \text{ kg m}^{-3}$ . Molecular dynamics simulations were performed on this new box in the NVT ensemble for 5 ns using PBC and the same cutoff distances as above. The temperature was once again maintained at 300 K using a Nosé-Hoover thermostat.

Over the last ns of this simulation, we gather 17 geometries to take into account the motion of the molecules during the charge transport phenomenon. On every geometry, we perform 400 MC simulations each lasting 10 000 ns. The results are then averaged.

We perform Monte Carlo simulations on all the systems assuming periodic boundary conditions. At every time step, a charge is situated on one of the 22 500 molecules composing the system and has certain probabilities to jump to one of its neighbor molecules. For each molecule, we consider 27 neighbors, those ones with edge-to-edge distance smaller than 7 Å. The hopping probabilities to all of these neighbors are calculated using Marcus formula

$$w_{if} = \frac{2\pi}{\hbar} |H_{if}|^2 \sqrt{\frac{1}{4\pi k_B T \lambda}} \exp\left(-\frac{(\Delta E_0 + \lambda)^2}{4\lambda k_B T}\right), \quad (13)$$

where  $\Delta E_0$  is the energy difference between the vibrational energies ground states of the two electronic levels considered and  $\lambda$  is the reorganization energy (Fig. 1(a)). In all the simulations, we fixed  $\lambda = 0.3 \text{ eV}^8$  and  $T = 300 \text{ K}$ . The molecular energy levels are obtained from an HF calculation on a perfect isolated 4PV molecule. From this calculation, we obtain 3 crucial quantities: (1) the orbitals energies, (2) the linear combination of orbitals coefficients weighting the  $p_z$ -orbitals located on the single C atoms, and (3) the charges present on C and H atoms in the 4PV ground state. All these quantities are used to calculate (13) as explained in the following.

For the transfer integrals  $H_{if}$ , we use a weighted Mulliken formula<sup>32</sup> for carbon atoms,<sup>33</sup> with the previously calculated orbital coefficients. This allows us to take into account the true off-diagonal disorder of the system.<sup>8</sup> The transfer integral is taken proportional to the molecular orbitals overlap that in turn is calculated on the basis of the overlap of the single atomic  $p_z$ -orbitals.

To conceptually link our simulations to theory, we decide to use a point dipole approximation. For every molecule, we calculate a point dipole, summing the atomic positions

weighted by the respective atomic charges. As pointed out in Sec. II, point dipoles are indeed the cause of Poole-Frenkel behavior at a macroscopic level. They surely introduce an approximation at the microscopic level, due to fact that the size of the molecules is comparable with the average intermolecular hopping distance, but local properties of the material are not the aim of this paper. Nevertheless, this simplified model will allow us in the following of this paper to relate our results with existing theoretical correlation models<sup>19,20</sup> and get some more insights on their validity.

As a further approximation, we assume that the atomic charges do not change with the different conformational arrangements in the box and we use the atomic charges obtained from the HF calculation on the isolated 4PV system. This assumption is motivated by computational reasons and we believe that the error introduced by this simplification does not affect our conclusions, qualitatively speaking.

The energy landscape of the system is of fundamental importance for our study. The energy of a molecular orbital,  $E_M$ , can be expressed as

$$E_M = \epsilon_M + \varphi_M, \quad (14)$$

where  $\epsilon_M$  is the orbital energy of the orbital  $M$  obtained from the HF calculation and  $\varphi_M$  is an energy shift for that orbital. For the purpose of this article, the energy shifts can be of two types leading to two classes of energy landscapes.

- Gaussian: The energy shift  $\varphi_M$  is a gaussian random variable  $\forall M$  with no spatial correlation introduced between different sites. The gaussian energy method is defined only in terms of the standard deviation  $\sigma$  for the DOS (gaussian- $\sigma$ ).

- Dipole correlation: The energy shift  $\varphi_M$  is a result of the interaction between the charge carrier occupying the orbital  $M$  and the nearby molecular dipoles (within a radius of 30 Å). From the output of the HF calculation, the dipole can be straightforwardly calculated for every molecule in the box, depending on the positions of its atoms in its particular conformation. A charge  $q$  on the molecular orbital  $M$  belonging to the  $i$ th molecule has an energy contribution (in cgs units)

$$\varphi_M = \sum_j \frac{\vec{p} \cdot q(\vec{r}_i - \vec{r}_j)}{\epsilon_r |\vec{r}_i - \vec{r}_j|^3}. \quad (15)$$

This contribution is the same for every orbital  $M$  of the  $i$ th molecule. Moreover, since the dipole of the 4PV molecule is very small ( $p_0 \simeq 0.09 \text{ D}$ ), we introduce an enhancement factor  $enh$  and we consider for the molecules a dipole of  $\vec{p} = enh \vec{p}_0$ ,

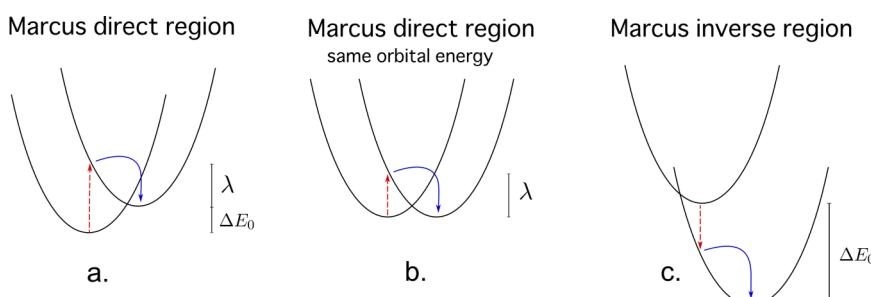


FIG. 1. Illustration of the different Marcus regions. Figures (a) and (b) represent the direct region in two different situations, while (c) represents the inverse Marcus region. In (c), the field is strong enough to reverse the direction of the transition (red arrows). From there on, increasing the field increases the energy difference between the two levels, making the charge transfer process more difficult.

with the purpose of increasing the effects of the dipoles on the energy landscape. This enhancement factor has no physical meaning but provides a theoretical degree of freedom, allowing us to study the importance of the diagonal disorder generated by a wider range of molecular dipoles. In this way, we can study the effect of different dipole magnitudes in an amorphous disordered structure 4PV-like. The nature of the correlation in the energetic landscape remains instead the same for every enhancement factor and the whole landscape is simply scaled by  $enh$ , as can be seen in (15). A dipole correlated energy method is thus defined in terms of its enhancement factor  $enh$  (dipole1, dipole2, etc.).

#### IV. RESULTS AND DISCUSSION

We built seven sets of systems on which we perform Monte Carlo simulations. Every set is composed of the 17 box geometries described in Sec. III. On two of these sets, we used the uncorrelated gaussian energy shifts with  $\sigma = 0.08$  eV and  $\sigma = 0.11$  eV, and on the other five, we used the dipole correlated energy shifts considering enhancement factors ( $enh$ ) of 2, 3, 4, 5, and 7. The values presented in the following are average values for each set, if not specified differently.

##### A. Sets properties

Several tools were developed to analyze the charge transport properties of the systems and to calculate their most important parameters. First of all, we can focus on the distribution of the energy levels. For uncorrelated systems, this is obviously a gaussian as imposed by the energy attribution procedure. A bit less obvious is that also the dipole correlated systems have a DOS which is a gaussian. An example of such a DOS for  $enh = 2$  is shown in (Fig. 2). This result is in agreement with the theoretically predicted DOS for randomly distributed dipoles.<sup>19</sup> The standard deviations for the DOS in these systems have been calculated for every set, with the results presented in Table I. It is worth remarking, as explained in Sec. III, that our dipoles are actually not randomly distributed, but they are, within the limitations of the approximations done, the dipoles given by the orientations of the molecules as obtained from the MD simulations. It can be interesting at this point to check the validity of the assumption (made, for example, in Ref. 19) that the dipoles in an amorphous material are independently and randomly distributed.

In Fig. 3, we present the average distribution of the cosine of the angle lying between two dipoles, in function of their distance. At low distances, this distribution is concentrated around some specific values of the cosine, different from 0 (Fig. 3(b)). Only few couples of molecules (around 10 per system) are closer than 3 Å, so this fact still gives an idea of dipoles arrangement but does not provide a good statistics. Above 5 Å instead we start having a statistically significant ensemble over which to calculate the average distribution of the cosine. We can notice that this distribution is initially (at 5 Å) more similar to a parabola (with higher values around 0 and  $\pi$  radians) meaning that dipoles locally have a lower probability to be orthogonal than to be aligned or in opposite

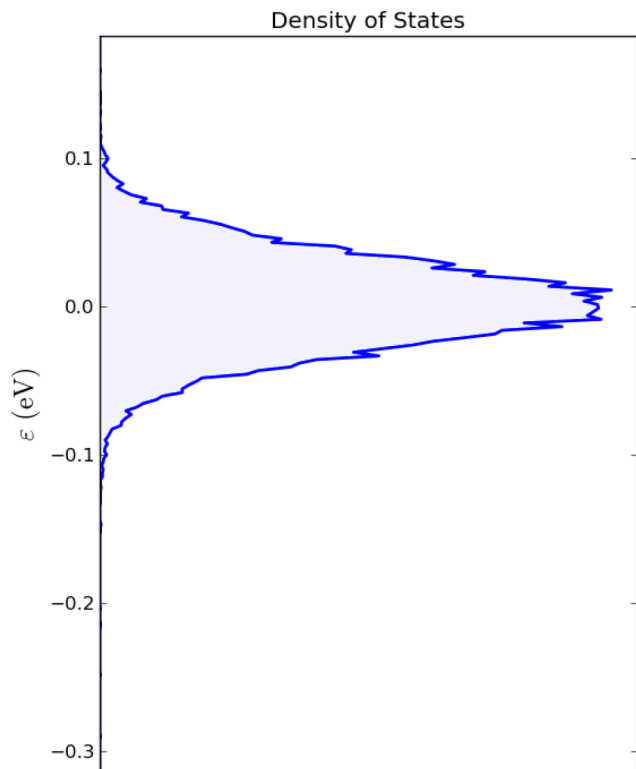


FIG. 2. Density of states of one system geometry with dipole2 diagonal disorder.

directions. Then with increasing distances, the distribution is progressively getting uniform validating the assumption of randomly distributed dipoles. This behavior minimizes the dipoles potential energy, as nearby dipoles will generally prefer to be in opposite directions. Of course this is not the only energy contribution determining the molecular packing and indeed even for really short distances we get two preferential cosine values that are not  $\pm 1$ . The tendency to avoid orthogonality anyway persists also at quite high distances ( $\sim 20$  Å) as can be seen in Fig. 3. This fact can be rationalized considering that when the molecular dipoles are orthogonal, the driving force, deriving from the derivative of the dipoles interaction energy, is maximum. In conclusion, the assumption of randomly distributed dipoles is true at high distances, while for short distances, there is a local orientational correlation between nearby molecular dipoles that could be an aspect to take into account in theoretical models.<sup>19,20</sup>

As pointed out above, we expect a substantially different behavior between systems built with the 2 different methods: gaussian and dipole correlated. An interesting characteristic to look at is the energy landscape; we expect the correlated energy landscape to be smoother than the uncorrelated. To visualize the energy landscape of a 3D system, we use the following approach. Starting from the first molecule in the box, we select from its neighbors those ones pointing "sufficiently" in the field direction. We require that the angle between the direction of the field and the direction of the vector connecting the two molecules fulfills  $\cos \vartheta > 0.7$ , i.e., we are moving inside a cone of  $\pi/4$ . Then, among these particular neighbors, we pick the nearest one and move there. Repeating this selection procedure for a fixed number of steps we have defined a chain

TABLE I. Parameters for the systems' sets with different energetic disorders.

Energy method	$\sigma$ (eV)	$A$ ( $\text{\AA}$ eV $^2$ )	$a_d$ ( $\text{\AA}$ )	$\zeta$ (eV)
gaussian-0.08	0.0800	...	...	0.113
gaussian-0.11	0.1100	...	...	0.155
dipole2	$0.0323 \pm 2 \times 10^{-4}$	$0.00280 \pm 7 \times 10^{-5}$	$2.7 \pm 1 \times 10^{-1}$	0.029
dipole3	$0.0484 \pm 3 \times 10^{-4}$	$0.0063 \pm 1 \times 10^{-4}$	$2.69 \pm 8 \times 10^{-2}$	0.043
dipole4	$0.0645 \pm 4 \times 10^{-4}$	$0.0112 \pm 3 \times 10^{-4}$	$2.7 \pm 1 \times 10^{-1}$	0.057
dipole5	$0.0809 \pm 2 \times 10^{-4}$	$0.0175 \pm 4 \times 10^{-4}$	$2.67 \pm 7 \times 10^{-2}$	0.073
dipole7	$0.1129 \pm 8 \times 10^{-4}$	$0.0343 \pm 8 \times 10^{-4}$	$2.7 \pm 1 \times 10^{-1}$	0.100

of molecules. In Fig. 4 is shown the energy landscape along this chain of molecules for the uncorrelated system with  $\sigma = 0.08$  eV and for the dipole correlated system with enhancement factor of 5 (these two systems have similar DOS, Table I).

The spatial correlation  $C(r) = \langle u(0)u(r) \rangle$  is also analyzed. Several values for the parameter  $a_d$  in (5) have been reported in the literature.<sup>34,35</sup> These estimates can be done for different types of regular lattices, but since in our case we have a disordered structure, we decide to use a numerical approach instead. As shown in Figure 4, the spatial correlation of the system with dipole energy shifts is in excellent agreement with the law  $1/r$  theoretically derived (5). With these data at hand, the proportionality parameter  $A = \sigma^2 a_d$  can be calculated for every dipole correlated system, taking the best fit to (5) in the range 5–10 Å. The choice of 5 Å as a lower limit is because the distance has to be sufficiently large to provide a statistically significant sample of nearest neighbors for every molecule. The higher limit of the range is somewhat arbitrary from a statistical point of view. As stated in Sec. III, we consider neighbors with edge distances within a radius of 7 Å, which corresponds approximately to a distance of 10 Å between the center of the molecules (where the dipoles are situated). We are thus interested in fitting the parameter  $a_d$  such that Eq. (5) will have the best agreement with our system in this range (5–10 Å).

The intrinsic energetic disorder of the system is represented by a parameter  $\zeta$ , defined as the average energy difference (in absolute value) between the orbitals of two nearest neighbor molecules,

$$\zeta \approx \sqrt{\langle (u(a) - u(0))^2 \rangle} = \sigma \sqrt{2 \left(1 - \frac{a_d}{a}\right)}, \quad (16)$$

which in fact is equal to  $\Sigma(a)$  from Eq. (6). Notice that we can use the same formula (16) for uncorrelated systems, setting  $a_d = 0$ .

The key parameters introduced above are summarized in Table I. There is also one additional parameter common to every system which is worth mentioning, the average distance between two neighboring molecules, which from the MD simulations, is determined to be  $a \approx 4.473 \pm 10^{-3}$  Å.

## B. Transition fields and working regions

Once our sets of systems have been built and analyzed, we can proceed with the Monte Carlo simulations to obtain the mobility. For each of 21 different electric field strengths in the range [0, 1.6e7] V/cm, we perform 400 MC simulations of 10 000 ns each. The extended simulation time is to ensure that the charge carrier has reached a steady transport state independent on the initial energy (i.e., the steady state of the Markov chain Monte Carlo). The results for each of the seven sets are presented in Fig. 5. The qualitative behaviour we obtain for the mobility field dependence (Fig. 5) is in accordance with experiments on organic materials.<sup>36–38</sup> In particular, we can notice that our simulations can reproduce the functional dependence of the mobility on the electric field better than a single analytical formula. Furthermore, opposed to Ref. 36,

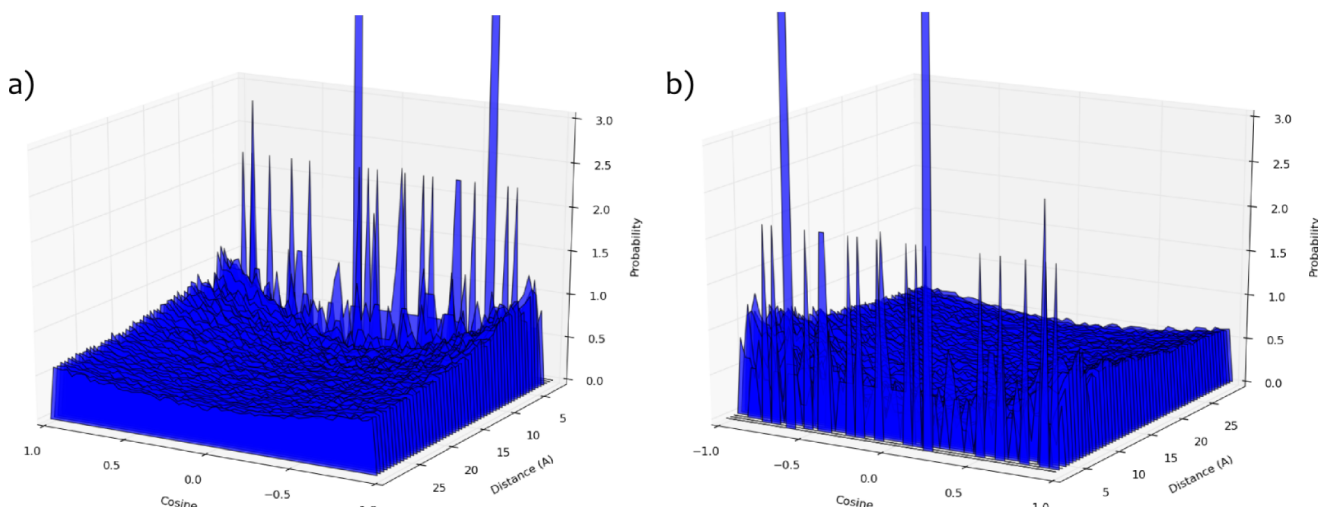


FIG. 3. Distribution of the cosine between nearby molecular dipoles in function of the distance, seen from two different angles.

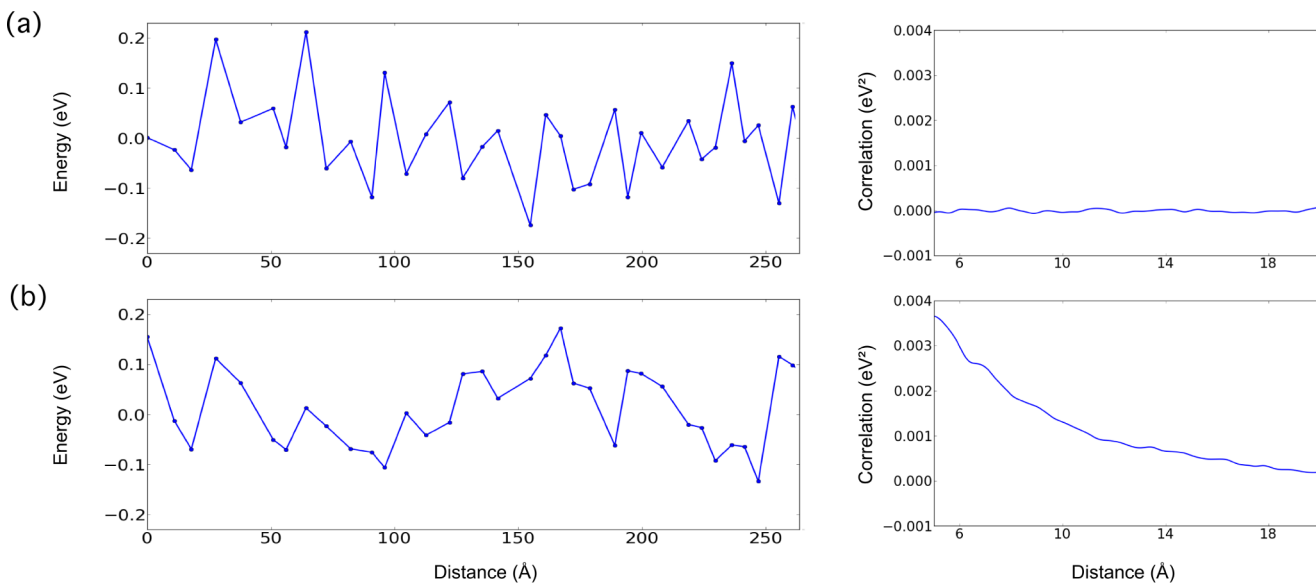


FIG. 4. Comparison between the energetic landscape of one system geometry with different types of diagonal disorder (a) uncorrelated gaussian with DOS  $\sigma = 0.08 \text{ eV}$  and (b) correlated dipole5. The right panel shows the respective statistical correlations calculated.

our model is based on Marcus formula which allows us to take into account reorganization effects in the material that we believe are important for organic compounds. Regarding the quantitative comparison with experiments, we are not aware of experimental data on PPV materials, but comparisons are possible with some PPV derivatives. Quantitatively results are not satisfactory<sup>39,40</sup> and it is difficult to say if this is due to a real difference in conduction of PPV derivatives or to some effect we are neglecting in our model (like material polarization and influence of intrachain transport in long PPV chains). However, there are parameters in our model that could be better calculated (higher level of theory for quantum mechanical calculations), or fitted to reproduce experimental data, but this is out of the scope of the present article.

It is clear from Fig. 5 that the functional dependence changes over the range of field strengths included in our study. At low field, all sets show a flat or inverse dependence. A possible explanation to this behavior could be the  $1/E$  term of (12) but, as we will show in the following of this section, this is not the case. In fact, decreasing the field below a certain value, the fundamental assumptions leading to (12) are no longer valid and we cannot use this expression to describe the mobility. The first region is the percolation region (Fig. 6). In this region, the energy gained by a charge carrier due to the presence of the electric field is low with respect to the disorder energy of the material and the dynamics can be well described by a percolation model. This behavior has been previously described in Ref. 21.

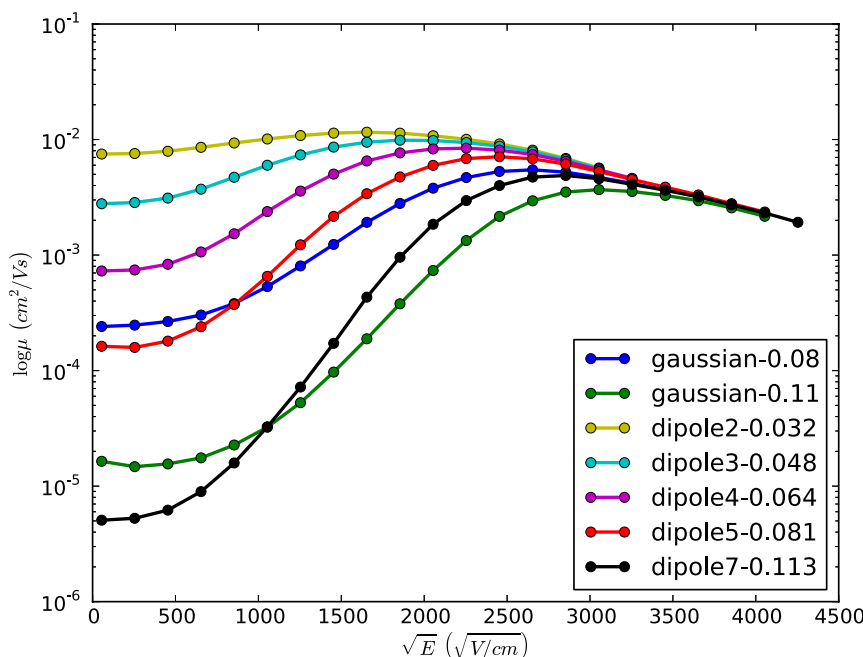


FIG. 5. Mobility field dependence for the different energy attribution methods. In the legend, following the name of the method, we report also the standard deviations of the DOS in eV.

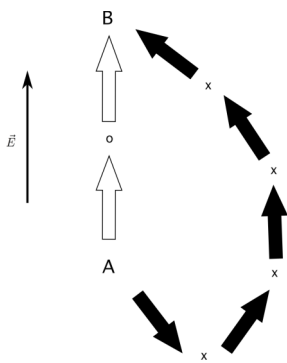


FIG. 6. Illustration of the role of the field in the disorder realm. The field assists the transport in the A-B direction, favoring the straight path for the charge. But when the system is energetically disordered, with hills on the way from A to B (point o), the most favorable path could instead be the one passing through the valleys on a side (points x). Adapted from Ref. 21.

At very high field strengths, we find the inverted Marcus region, the field is sufficiently high to reverse the position of the crossing of the two parabolas (Fig. 1(c)). In this region, as expected, we obtain a decrease of the mobility with increasing field.

As previously discussed (see Sec. II), in between these two regions we expect the correlation region, i.e., the region where (5) is valid. Since we have two regimes with non-linear behavior, one for weak field strengths and one for high field strengths, it will always be possible to identify a range in between where to find a linear behavior for the mobility dependence. This is what is generally done when the Poole-Frenkel mobility dependence is experimentally identified. In this work, instead, we want to understand how to determine the position of these different regions on the field strength axis for every given material. First of all, we need to identify the position of the correlation region and to address this issue, let us first determine those field strengths at which we theoretically expect transitions in the conduction behavior.

A first transition is determined by the disorder of the system, which is strongly related to the correlation of the energy landscape. For the field  $E$  to affect the energy landscape, i.e., to play a more evident role in the conduction than causing a drift of the charge carrier, its effect has to result in a shift of the molecular energetic parabolas (Fig. 1) not negligible compared to the intrinsic disorder. We are thus in the percolation region if the field fulfills  $e\vec{E} \cdot \vec{d} \ll \zeta$  and the contribution of the field to the energy landscape is too small to produce any effect on the mobility. Then taking the “ $\ll$ ” sign as “one order of magnitude smaller,” we argue that for electric fields larger than

$$E_{Id} = \frac{1}{10} \frac{\zeta}{ea}, \quad (17)$$

the previous inequality does not hold anymore. We take  $E_{Id}$  as the transition field at which the conduction mechanism starts to deviate from the percolation model (not a sharp transition in this case). The  $d$  in the subscript stands for disorder, since this is the transition field given by the intrinsic disorder, and  $I$  refers to the fact that the transition happens before the correlation region. Opposed to the index  $II$  that we will use below for the transition fields happening after the correlation region.

When the field is strong enough, there is a transition into the inverse Marcus region (Fig. 1(c)). This transition occurs when

$$\Delta E_0 = \zeta - e\vec{E} \cdot \vec{a} \simeq -\lambda. \quad (18)$$

Let us consider the field  $E_i$ ,

$$E_i \simeq \frac{(\lambda + \zeta)}{ea}. \quad (19)$$

The sign of  $\zeta$  is taken concordant with  $\lambda$ , to make sure that the inverse Marcus condition applies to the majority of adjacent pairs of molecules. If we indeed look at what happens at this field in Fig. 5, we notice that the material is already in the inverse linear zone. To have an idea of where the transition instead should be, we decide to divide this field by 2, thus finding ourselves at lower field strengths for which the inverse effects completely rule the conduction, but sufficiently near to the point in which they become important. The transition field to the inverse Marcus region is then taken as

$$E_{IIi} = \frac{1}{2} \frac{(\lambda + \zeta)}{ea}, \quad (20)$$

where the  $i$  in the subscripts stands for inverse zone.

It is clear from our results (Fig. 5) that at high fields the disorder of the material is of no importance for the transport properties and all the curves collapse into one. This is a clear effect of the inverted Marcus regime (Fig. 1), where the parabolae of two neighboring molecules are shifted with respect to each other to such an extent that the initial diagonal disorder has no effect on the transfer rates. It should be mentioned that the high-field non-linearity presented here originates from a different mechanism compared to a similar observation made from simulations based on the Miller-Abrahams transfer rate.<sup>41</sup> In this case, a velocity saturation effect is obtained at high field strengths due to the field independent transfer rates along the dominating transport direction.

Between the percolation and the inverted region lies the correlation region, a region in which the correlation relating width and depth of the traps determines the functional dependence of the mobility (see Sec. II). Indeed as soon as the field increases, the correlation is taking part in the transport process. As we recall from (10), when the field tends to 0, the critical radius tends to infinity. However, the material in which the transport is taking place has a finite extent and thus there is an upper limit to the possible width of its traps. The correlation then introduces a transition at low fields, when the critical trap width  $r_c$  exceeds the material length  $L$  in the direction of the field, i.e., when  $2r_c = L = 24$  nm (since our field is in z direction). At this point, the critical traps with radius expressed by (10) are not present in the material and (12) is no more valid, failing the assumptions leading to it. From (10), we then get the expression for the low field correlation transition to be

$$E_{Ic} = \frac{4A}{ek_BTL^2}. \quad (21)$$

It is worth noticing that the transition expressed by (21) is valid only for the specific correlation given by dipoles (5), but the same procedure is applicable to any kind of correlated energy landscape. In the uncorrelated case (with  $\langle u(0)u(r) \rangle = 0$ , implying  $A = 0$ ), the critical traps are always the most narrow

TABLE II. Theoretically predicted transition fields (in  $\sqrt{V/cm}$ ) for systems with different energetic disorders (see also Fig. 5).

Energy method	$\sqrt{E_{Id}}$	$\sqrt{E_{Ic}}$	$\sqrt{E_{IIIi}}$	$\sqrt{E_{IIc}}$
gaussian-0.08	502.92	...	2148.98	...
gaussian-0.11	589.73	...	2256.63	...
dipole2	253.56	27.42	1917.01	735.75
dipole3	310.83	41.14	1958.70	1103.63
dipole4	358.31	54.85	1998.85	1471.51
dipole5	402.98	68.56	2040.93	1839.39
dipole7	474.06	95.99	2115.92	2575.14

and deep independently on the field, and the above formula gives us consistently  $E_{Ic} = 0$ . Still for correlated systems, an additional problem can happen at high fields instead. Considering (10), if the field keeps increasing, the critical radius can become smaller than the intermolecular separation  $a$ , which again is inconsistent with the assumptions leading to (12). The high field correlation transition then happens when  $r_c = a$ , i.e., when the critical radius is equal to the average distance from the neighbors of the first shell

$$E_{IIc} = \frac{A}{ek_B T a^2}. \quad (22)$$

In Table II, we report the transition fields for all of the systems included in our studies.

Let us recall that dipole5 and dipole7 have DOS standard deviations ( $\sigma$ ) that are close to the values of gaussian-0.08 and gaussian-0.11, respectively. This point will allow us to study the role of correlation in the electric field dependence of the mobility. In particular, let us take a look at Fig. 7(a) in which we compare dipole7 with gaussian-0.11, enlightening all the transitions occurring. We can identify the following three regions.

- The percolation region, before the Id transition. This first region is the realm of disorder, the field strength is very small and the percolation model works well (we can notice this behavior also in Ref. 21, Fig. 8).
- The correlation region. This region lies above  $\max(E_{Id}, E_{Ic})$ , i.e., when we are out of the percolation region and the critical radius is small enough compared to the system length, and below  $\min(E_{IIc}, E_{IIIi})$ , i.e., when the critical radius is large compared to the typical intermolecular separation and the inverse Marcus effects are not excessively relevant yet. The specific functional dependence in this region is determined by the particular type of energy correlation, typically Poole-Frenkel behavior (12) is observed for polar materials, but also other behaviors are possible for other types of molecular electrostatic interactions in the material (e.g., quadrupoles and octupoles).<sup>14</sup>
- The inverse region, above the  $E_{IIIi}$  transition field. This region shows an inverse dependence of the mobility on the field, inherited by the inverse Marcus region between two neighboring molecules.

Looking at Fig. 7(b), we can notice that the correlation caused by the electric dipoles introduced in our system produces a linear behavior in the correlation region, while the uncorrelated curves present a more quadratic behavior, as theoretically expected from (12).

In conclusion, once the key parameters of a material are given, it is possible to successfully identify the transition fields and thus to locate the position of the different regions.

### C. Trap analysis

A lot of information concerning the details of the charge transport can be extracted from the data produced during the

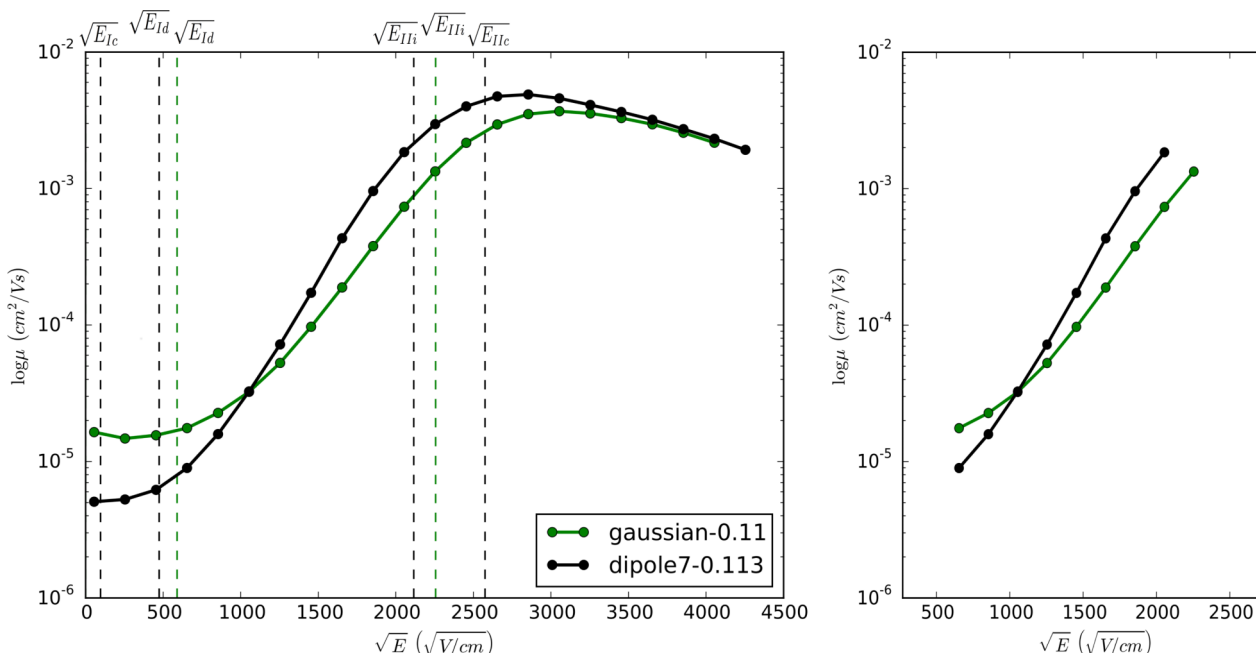


FIG. 7. Mobility field dependence and transitions for the dipole7 and gaussian-0.11 energy attribution methods. The right panel shows a plot of the correlation region alone.

simulations. In particular, since the modeling is performed at the molecular level, we can analyze important statistics per molecule like the average dwell time and the number of hops. For every molecule and for every simulation, we store the number of time the hole hops to a particular molecule (*nhops*) and the total time the charge carrier spends on that molecule (*cumdwelldtimes*). The average dwell time at the end of the simulation is simply the average

$$\text{dwelltime} = \frac{\text{cumdwelldtimes}}{\text{nhops}}. \quad (23)$$

In Figure 8(c), as an example for illustration purposes, we can see one system geometry with energy attribution method dipole7 and field  $4.2 \times 10^6$  V/cm. The molecules are colored on the basis of the dwell times in the simulation, to be able to visually identify the traps. The scale is from red (0 ps) to blue (20 ps), passing through white. The single site traps in a material are those molecules for which the dwell time is

particularly high. They can be identified from the tail of the dwell time distribution in (Fig. 8(a)). With the increasing field, we notice that the trap population shrinks and the single site traps become progressively less important. This happens until a certain field when the inverse Marcus region effects take place and we notice a reverse tendency. Single site traps are mainly due to diagonal disorder (molecular energy difference) and they affect the  $\Delta E_0$  term in Marcus formula (13).

Let us then focus on the evolution of the number of hops (Fig. 8(b)). At low field strengths (below  $5\text{--}6 \times 10^6$  V/cm), the peak in the distribution is centered on a small number of hops (some hundreds). This peak is wider and shifted on higher number of hops for higher field strengths, when more preferential channels for the charge carriers become active. Consequently, there will be more hops to the molecules in these channels which explains the, in general, larger values of *nhops* with increasing field strength. Moreover, based on the *nhops* statistics, we can also identify traps of a different kind than

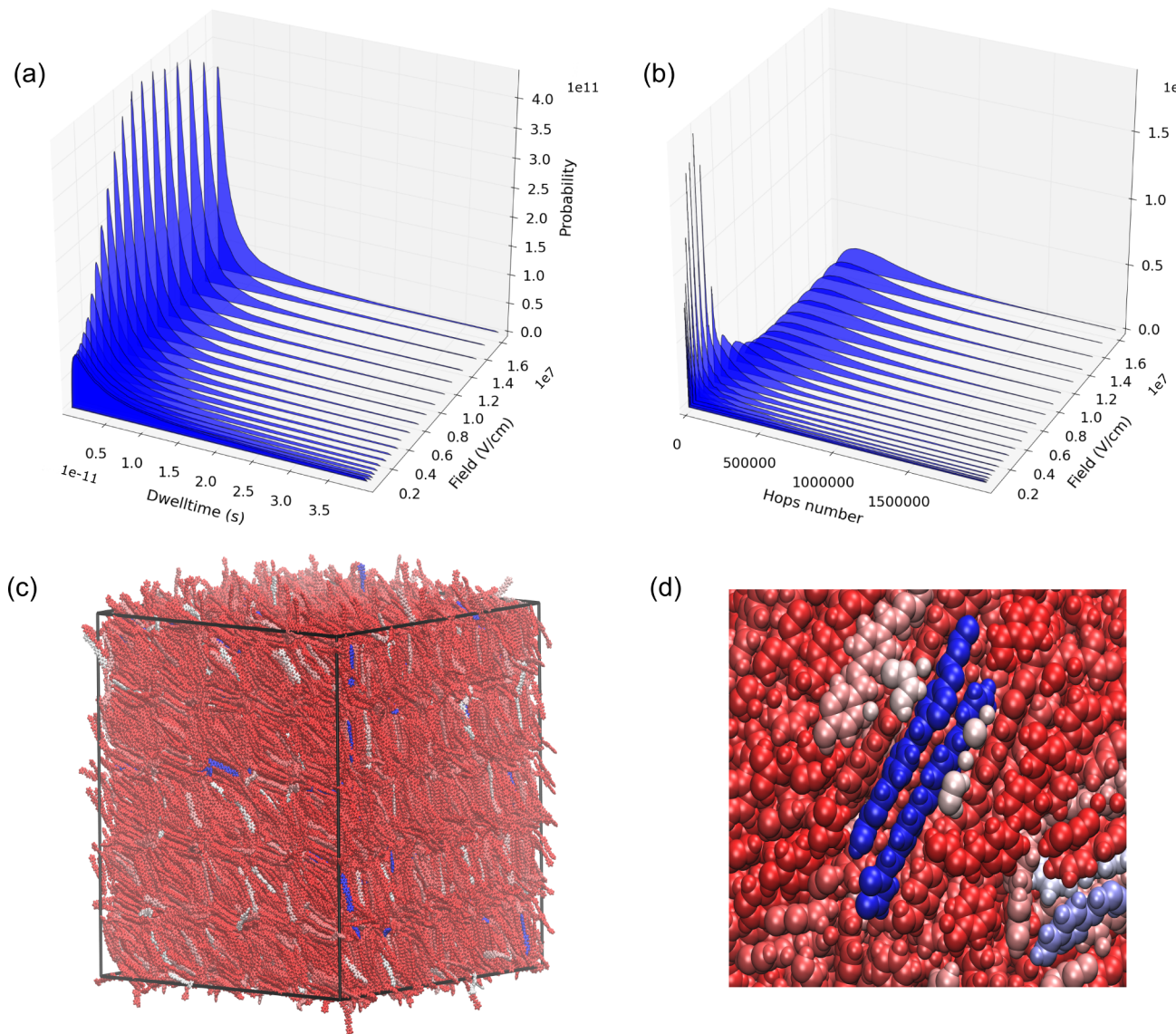


FIG. 8. Traps analysis for one system geometry: (a) distribution of dwell times and (b) distribution of the number of hops per molecule. A visualization of the system is shown in (c), the molecules are colored on the basis of their dwell times, from red (0 ps) to blue (20 ps), passing through white. The colors in figure (d) are instead dependent on the number of hops, still following the red-white-blue color scale.

the single molecule traps. These traps are mainly due to off-diagonal disorder, more specifically to variations in the  $H_{ij}$  term of (13). In Fig. 8(d) is shown a close up of the same system of Fig. 8(c) but the molecules are now colored on the basis of the number of hops. The molecules with the largest number of hops are displayed in blue. The figure shows a pair of closed lying  $\pi$ -stacked neighboring molecules, both with a high number of hops. We refer to this as a resonant dimer trap, the charge carrier jumps back and forth, resonating between these two molecules and remaining trapped in that region.

This kind of traps resembles to some extent the incipient dimer trap hypothesized as one of the possible kinds of dislocation traps in anthracene crystals.<sup>42</sup> The incipient dimer is seen as a pair of anthracene molecules with separation distances smaller than the equilibrium distance, forming a lower energy level delocalized over the two molecules. In our model instead, the electron is allowed to be delocalized only over a single molecule and the trapping mechanism is arising from the strong intermolecular interactions between the two molecules. These two pictures are anyway inseparable and they reflect the same mechanism from two different points of view, two different bases for the hamiltonian matrix. Another way of expressing this is that we work with a non-diagonalized hamiltonian (molecular energies of the single molecules and transfer integrals between them) and not with a diagonalized one (energies of the states delocalized over the whole dimer). Consequently, in this model, only the single site traps are arising from the diagonal disorder of the system (variations in the energy landscape), while the dimer traps are arising mainly from the off-diagonal disorder.

In more strongly packed material, we can also imagine the formation of grain traps, generalization of a dimer trap to multiple molecules well coupled among themselves. When studying the conduction in a new kind of material, it is important to be aware of the fact that also off-diagonal disorder can generate traps that generally are not visible from the single molecular dwell time distribution (Fig. 8(a)). Remarkably, a well ordered region in a disordered material is indeed a trap.

In this study, we vary only the diagonal disorder through the molecular dipoles and let the structure of the material and therefore also the off diagonal disorder remains the same in all simulations. Thus, we are not comparing the two types of disorder in terms of which of them is the limiting factor for charge transport. A more strongly structurally disordered material will naturally exhibit a lower mobility and shift all curves in Fig. 5 downwards on the vertical scale. The methodology introduced here can in principle be used to study this effect, but in this case, the structures have to be created artificially instead of taken directly from MD simulations as has been the method chosen for this study.

## V. CONCLUSIONS AND PERSPECTIVES

We have presented a Monte Carlo model used to simulate disordered PPV for a range of electric fields [ $0, 1.6 \times 10^7$ ] V/cm, allowing us to gain some theoretical understanding on the field dependence of the charge carrier mobility. The field dependence cannot be expressed through a single analytical formula, the behavior of the material is separated

in three different working regions: the percolation region, the correlation region, and the inverse Marcus region. The theoretical transition fields between these regions have been identified and discussed, allowing us to predict for a given material the mobility field dependence for a broad range of electric fields.

Several tools have been developed to analyze important properties of organic systems, in particular the DOS, a realistic angular distribution for the molecular dipoles and the energy landscape which also includes the spatial correlation and the disorder. The modeling was performed at the molecular level which allows us to perform trap analysis, studying the distributions of dwell time and number of hops per molecule. From this type of analysis, we have been able to identify the traps for charge transport that are due to diagonal as well as off diagonal disorder. In particular, the number of hops in the simulation could be used to identify the grain traps, a more complex type of traps strongly connected to off diagonal disorder. We are confident that this study paves the way to establish the relation between morphology and efficiency in organic devices. The trap analysis so far presented can be pushed further to study the supramolecular organization in organic materials. We believe that these tools will become useful in addressing problems like how to improve mobility in the single phase of organic devices or how interface morphology affects efficiency in organic solar cells.

## ACKNOWLEDGMENTS

Financial support from the Swedish Research Council (VR) and computational resources and support from the MATTER Network is gratefully acknowledged. M.L. thanks SERC (Swedish e-Science Research Center) for funding and SNIC (Swedish National Infrastructure for Computing) for providing computer resources.

- <sup>1</sup>J. Wang, F. Zhang, J. Zhang, W. Tang, A. Tang, H. Peng, Z. Xu, F. Teng, and Y. Wang, "Key issues and recent progress of high efficient organic light-emitting diodes," *J. Photochem. Photobiol., C* **17**, 69-104 (2013).
- <sup>2</sup>D. Wohrle and D. Meissner, "Organic Solar Cells," *Adv. Mater.* **3**, 129 (1991).
- <sup>3</sup>J. Garland, T. Biegala, M. Carmody, C. Gilmore, and S. Sivananthan, "Next-generation multijunction solar cells: The promise of II-VI materials," *J. Appl. Phys.* **109**, 102425 (2011).
- <sup>4</sup>X. Guo, M. Baumgarten, and K. Müllen, "Designing  $\pi$ -conjugated polymers for organic electronics," *Prog. Polym. Sci.* **38**, 1832 (2013).
- <sup>5</sup>L. Muccioli, G. D'Avino, R. Berardi, S. Orlandi, A. Pizzirusso, M. Ricci, O. Roscioni, and C. Zannoni, "Supramolecular organization of functional organic materials in the bulk and at organic/organic interfaces: A modeling and computer simulation approach," *Topics in Current Chemistry* (Springer, 2013), pp. 1–63.
- <sup>6</sup>R. A. Marcus, "On the theory of oxidation-reduction reactions involving electron transfer. I," *J. Chem. Phys.* **24**, 966 (1956).
- <sup>7</sup>C. Andrieu, A. Doucet, and R. Holenstein, "Particle Markov chain Monte Carlo methods," *J. R. Stat. Soc. B* **72**, 269 (2010).
- <sup>8</sup>M. Jakobsson, M. Linares, and S. Stafström, "Monte Carlo simulations of charge transport in organic systems with true off-diagonal disorder," *J. Chem. Phys.* **137**, 114901 (2012).
- <sup>9</sup>J. Brédas, D. Beljonne, V. Coropceanu, and J. Cornil, "Charge-transfer and energy-transfer processes in pi-conjugated oligomers and polymers: A molecular picture," *Chem. rev.* **104**, 4971 (2004).
- <sup>10</sup>V. Lemaur, D. da Silva Filho, V. Coropceanu, M. Lehmann, Y. Geerts, J. Piris, and J. Cornil, "Charge transport properties in discotic liquid crystals: A quantum-chemical insight into structure-property relationships," *J. Am. Chem. Soc.* **126**, 3271 (2004).

- <sup>11</sup>Y. Olivier, V. Lemaur, J. Brédas, and J. Cornil, "Charge hopping in organic semiconductors: Influence of molecular parameters on macroscopic mobilities in model one-dimensional stacks," *J. Phys. Chem. A* **110**, 6356 (2006).
- <sup>12</sup>F. Castet, P. Aurel, A. Fritsch, L. Ducasse, D. Liotard, M. Linares, and D. Beljonne, "Electronic polarization effects on charge carriers in anthracene: A valence bond study," *Phys. Rev. B* **77**, 115210 (2008).
- <sup>13</sup>J. Frenkel, "On pre-breakdown phenomena in insulators and electronic semiconductors," *Phys. Rev.* **54**, 647 (1938).
- <sup>14</sup>S. Novikov, "Hopping charge transport in organic materials," *Russ. J. Elektrochim.* **48**, 388 (2012).
- <sup>15</sup>S. Novikov, D. Dunlap, V. Kenkre, P. Parris, and A. Vannikov, "Essential role of correlations in governing charge transport in disordered organic materials," *Phys. Rev. Lett.* **81**, 4472 (1998).
- <sup>16</sup>Y. Garstein and E. Conwell, "High-field hopping mobility in molecular systems with spatially correlated energetic disorder," *Chem. Phys. Lett.* **245**, 351 (1995).
- <sup>17</sup>D. Dunlap, P. Parris, and V. Kenkre, "Charge-dipole model for the universal field dependence of mobilities in molecularly doped polymers," *Phys. Rev. Lett.* **77**, 542 (1996).
- <sup>18</sup>D. Dunlap, V. Kenkre, and P. Parris, "What is behind the  $\sqrt{E}$ ?", *J. Imag. Sci. Tech.* **43**, 437 (1999).
- <sup>19</sup>S. Novikov and A. Vannikov, "Distribution of electrostatic potential in a lattice of randomly oriented dipoles," *JETP* **79**, 482 (1994).
- <sup>20</sup>S. Novikov and A. Vannikov, "Cluster structure in the distribution of the electrostatic potential in a lattice of randomly oriented dipoles," *J. Phys. Chem.* **99**, 14573 (1995).
- <sup>21</sup>H. Bässler, "Charge transport in disordered organic photoconductors, a Monte Carlo simulation study," *Phys. Status Solidi B* **175**, 15 (1993).
- <sup>22</sup>W. Jorgensen and J. Tirado-Rives, "The OPLS [optimized potentials for liquid simulations] potential functions for proteins, energy minimizations for crystals of cyclic peptides and crambin," *J. Am. Chem. Soc.* **110**, 1657 (1988).
- <sup>23</sup>W. Jorgensen, D. Maxwell, and J. Tirado-Rives, "Development and testing of the OPLS all-atom force field on conformational energetics and properties of organic liquids," *J. Am. Chem. Soc.* **118**, 11225 (1996).
- <sup>24</sup>B. Hess, C. Kutzner, D. van der Spoel, and E. Lindahl, "GROMACS 4: Algorithms for highly efficient, load-balanced, and scalable molecular simulation," *J. Chem. Theory Comput.* **4**, 435 (2008).
- <sup>25</sup>D. van der Spoel, E. Lindahl, B. Hess, G. Groenhof, A. Mark, and H. Berendsen, "GROMACS: Fast, flexible, and free," *J. Comput. Chem.* **26**, 1701 (2005).
- <sup>26</sup>E. Lindahl, B. Hess, and D. van der Spoel, "GROMACS 3.0: A package for molecular simulation and trajectory analysis," *J. Mol. Model.* **7**, 306 (2001).
- <sup>27</sup>H. Berendsen, D. van der Spoel, and R. van Drunen, "GROMACS: A message-passing parallel molecular dynamics implementation," *Comput. Phys. Commun.* **91**, 43 (1995).
- <sup>28</sup>S. Nosé, "A molecular dynamics method for simulations in the canonical ensemble," *Mol. Phys.* **52**, 255 (1984).
- <sup>29</sup>W. G. Hoover, "Canonical dynamics: Equilibrium phase-space distributions," *Phys. Rev. A* **31**, 1695 (1985).
- <sup>30</sup>M. Parrinello and A. Rahman, "Polymorphic transitions in single crystals: A new molecular dynamics method," *J. Appl. Phys.* **52**, 7182 (1981).
- <sup>31</sup>S. Nosé and M. Klein, "Constant pressure molecular dynamics for molecular systems," *Mol. Phys.* **50**, 1055 (1983).
- <sup>32</sup>R. Mulliken, C. Rieke, D. Orloff, and H. Orloff, "Formulas and numerical tables for overlap integrals," *J. Chem. Phys.* **17**, 1248 (1949).
- <sup>33</sup>A. Hansson and S. Stafström, "Intershell conductance in multiwall carbon nanotubes," *Phys. Rev. B* **67**, 075406 (2003).
- <sup>34</sup>D. Dunlap and S. Novikov, "Charge transport in molecularly doped polymers: A catalogue of correlated disorder arising from long-range interactions," *SPIE* **3144**, 80 (1997).
- <sup>35</sup>S. Novikov, D. Dunlap, and V. Kenkre, "Charge carrier transport in disordered organic materials: Dipoles, quadrupoles, traps, and all that," *SPIE* **3471**, 181 (1998).
- <sup>36</sup>B. Hartenstein, H. Bässler, S. Heun, P. Borsenberger, M. van der Auweraer, and F. de Schryver, "Charge transport in molecularly doped polymers at low dopant concentrations: Simulation and experiment," *Chem. Phys.* **191**, 321 (1995).
- <sup>37</sup>V. Kažukauskas, M. Pranaitis, L. Sicot, and F. Kajzar, "Negative mobility dependence on electric field in poly(3-alkylthiophene)s," *Mater. Sci.* **12**, 187 (2006).
- <sup>38</sup>B. Limketkai, P. Jadhav, and M. Baldo, "Electric-field-dependent percolation model of charge-carrier mobility in amorphous organic semiconductors," *Phys. Rev. B* **75**, 113203 (2007).
- <sup>39</sup>C. Vijila, B. Balakrishnan, C. Huang, Z. Chen, C. Zhen, M. Auch, and S. Chua, "Non-dispersive hole transport in a novel trifluoromethyl-biphenyl substituted PPV derivative," *J. Phys.: Conf. Ser.* **28**, 53 (2006).
- <sup>40</sup>S. Quan-Min, H. Yan-Bing, L. Jing, J. Hui, and L. Yun-Bai, "Hole transport properties of MEH-PPV at different excitation wavelengths," *Chin. Phys. Lett.* **23**, 950 (2006).
- <sup>41</sup>S. Raj Mohan, M. Singh, and M. Joshi, "Negative field dependence of mobility in disordered organic thin films due to non-equilibrium charge transport," *Org. Electron.* **11**, 1642 (2010).
- <sup>42</sup>G. Owen, J. Sworakowski, J. Thomas, D. Williams, and J. Williams, "Carrier traps in ultra-high purity single crystals of anthracene," *J. Chem. Soc., Faraday Trans. 2* **70**, 853 (1974).